Theor Chem Acc (2006) 116: 183–193
DOI 10.1007/s00214-005-0004-1

REGULAR ARTICLE

Arjan van der Vaart

Simulation of conformational transitions

Received: 5 April 2005 / Accepted: 28 July 2005 / Published online: 10 January 2006

Abstract Conformational transitions are essential for the functioning of many proteins, and understanding this dynamical behavior is a central goal in molecular biology. Computer simulations are playing an important role towards this aim by providing insights into how the conformational changes are induced, propagated and used. Popular methods for the simulation of conformational transitions will be reviewed, with a focus on atomistic molecular dynamics techniques for the calculation of transition pathways.

Keywords Conformational change · Simulation · Molecular dynamics

1 Introduction

The first observation of a conformational change occurred in 1938, when Felix Haurowitz [1] witnessed the transformation of hexagonal deoxyhemoglobin crystals into elongated prismatic forms upon oxygenation. His startling discovery showed that native hemoglobin is not a static molecule; instead, it adopts different conformations during and part of its functional cycle. This intimate connection between protein dynamics and function has been observed for many more proteins since. In fact, conformational changes are crucial for the functioning of many transport proteins (e.g., hemoglobin [2] and the periplasmic binding proteins [3]) and also for the catalytic process of many enzymes (e.g., for dihydrofolate reductase [4,5]). Moreover, conformational changes are essential in the molecular mechanism of protein regulation (e.g., in hemoglobin [2], protein kinases [6] and in voltage-gated, ligand-gated and mechanosensitive ion channels [7–9]), as well as responsible for the conversion of chemical energy into mechanical work in motor proteins (e.g., in myosin, kinesin and dynein [10,11], F_1-ATPase [12] and GroEL [13,14]).

A. van der Vaart
Department of Chemistry and Chemical Biology,
Harvard University, 12 Oxford Street, Cambridge, MA 02138, USA
E-mail: vaart@fas.harvard.edu

The conformational change is often involved in the coupling of two or more ligand binding sites (allostery) [15,16]. The coupling can be cooperative, meaning that successive ligands are bound with increasing affinity (e.g., for oxygen binding to hemoglobin [2]), or anti-cooperative, meaning that for successive ligands, there is a decreasing affinity (e.g., for tyrosyl binding to tyrosyl-tRNA synthetase [17]). A particularly interesting allosteric system is the GroEL chaperone, which consists of two seven-membered rings (Fig. 1a, b). ATP binds cooperatively to members within a ring but anti-cooperatively to members of different rings [18]. Not all conformational changes give rise to allosteric effects: in catalysis, a conformational change often closes a binding site, which traps the substrate and properly positions the catalytic groups (e.g., in triosephosphate isomerase [19]).

Most of the structural information on conformational transitions comes from X-ray crystallography [20]. Spatial information on the location and extent of a conformational change may be obtained from a comparison of protein structures with and without bound effector molecules. It can also be obtained from a comparison of structures that are crystallized in different buffers or that crystallize in different crystal groups. Lastly, it may be found by comparing the structures in a single unit cell if the cell is occupied by more than one molecule. Cryo-electron microscopy (EM) is also very useful for the study of conformational changes [21,22]. Although the resolution of most EM studies is of the order of 10 Å, atomic resolution models may be built if X-ray data exists for isolated fragments of the protein. The calculated electron density of the assembled fragments can then be fit to the experimental density, assuming that the orientation and position of the subunits can be obtained from rigid body displacements. Of special interest is the single-particle imaging technique, in which EM is used to study proteins that are trapped in different conformational states [22]. A third important experimental technique is nuclear magnetic resonance (NMR) [23,24]. In addition to structural information at atomic resolution, NMR can yield important dynamical information relevant to conformational changes. Dynamical information is also obtained with the recently developed time-resolved X-ray diffraction

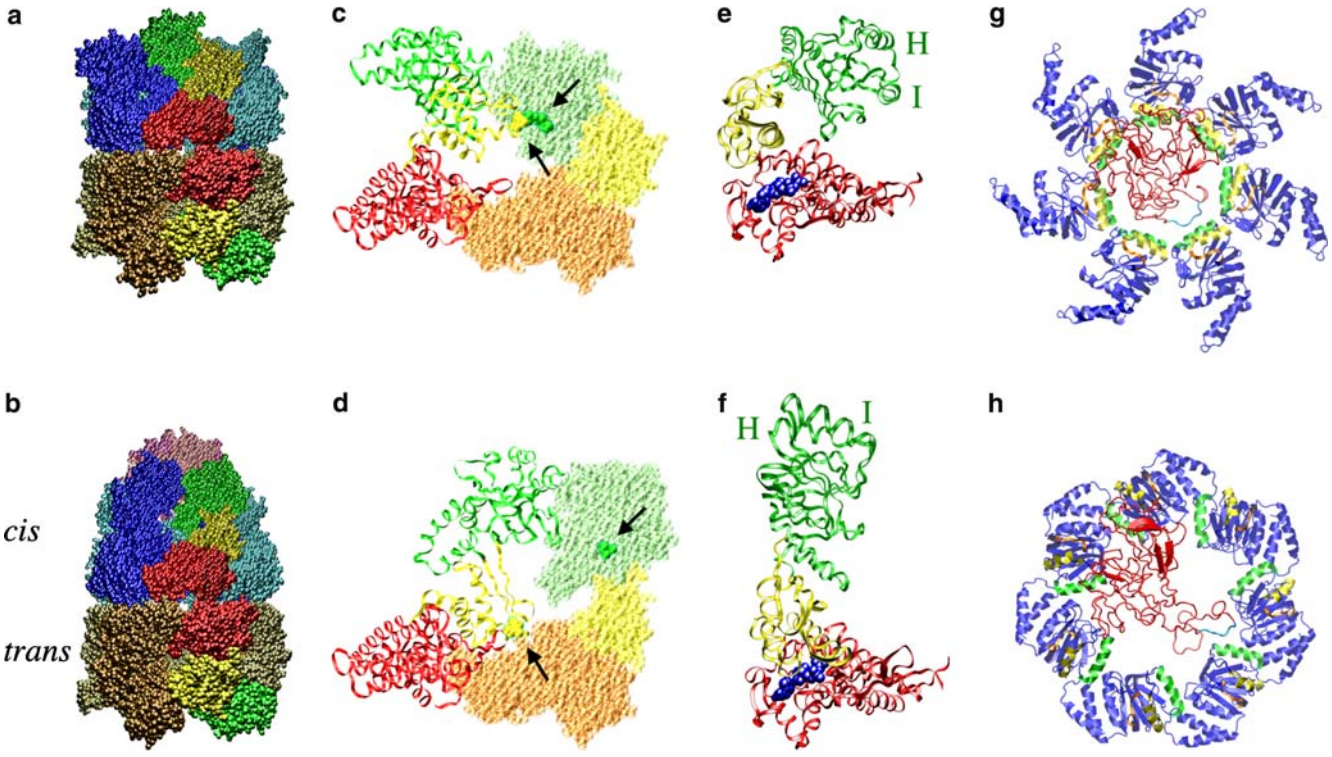

Fig. 1 Conformational states of the GroEL chaperone. **a** The closed (t) state consists of two identical seven-membered rings that each enclose a central cavity [97, 108]. Each chain has three domains: an equatorial domain (*red*), an intermediate domain (*yellow*) and an apical domain (*green*). **b** In the open (r″) state, ATP and the co-chaperone GroES (shown in *pink*) bind to the *cis* ring. The *cis* ring is enlarged, with a twofold increase of the volume of the cavity, while the *trans* ring remains in the closed conformation [98]. **c** The intra-ring, intersubunit contacts in the closed state involve a salt bridge (indicated by the *arrows*) between Glu386 of the intermediate domain (*yellow*) and Arg197 of the neighboring apical domain (*green*). **d** In the *cis* ring of the open state, the Glu386–Arg197 salt bridge is broken. The orientation of **c** and **d** is slightly different than that of **a** and **b** to highlight the position of Glu386 and Arg197. The orientation of the equatorial domains of **c** and **d** is identical. **e** Chain structure in the closed state. ADP (*blue*) is bound to the equatorial domain; the H and I helices of the apical domain point towards the inside of the cavity. **f** Chain structure of the *cis* ring in the open state. ATP is shown in *blue*; the H and I helices are at the *top* of the cavity and bind GroES. The chains in **e** and **f** have been rotated by 90° with respect to **a** and **b**; the cavity is on the *right-hand side* for **e** and **f**. **g** The binding of denatured rhodanese to the apical domains of the closed state *cis* ring [14]. The system is viewed from the top, down into the cavity. The H helices are shown in *yellow*, the I helices in *green*, the loops formed by residues 310-315 (which, like the H and I helices, were important for substrate binding) in *orange*, the rest of the apical domains in *blue*. Rhodanese is shown in *red*, except for the loop consisting of residues 45–50 which is shown in *blue*. This loop was tightly bound to the H and I helices of one of the apical domains. **h** The binding of denatured rhodanese to the apical domains of the half open (r′) state at the end of the TMD simulation [14]. Rhodanese became more unfolded during the closed to r′ transition of GroEL. The figure was prepared with VMD [109] and POV-Ray (http://www.povray.org).

techniques [25, 26], which solve the atomic structure at short time intervals (∼100 ps). Experimental techniques that give more limited (lower resolution) structural information on conformational changes include circular dichroism, fluorescence, infrared and Raman spectroscopies [27], single molecule atomic force microscopy [28, 29], single molecule spectroscopy [30, 31] and small angle X-ray scattering [20, 32].

There is a wide variety in the magnitude, type and time scale of conformational transitions. Atoms may be displaced by a few angstrom (as in dihydrofolate reductase [33]) or by as much as 100 Å (as in the pH-induced conformational change of hemagglutinin [34]). Analyses of X-ray structures have shown that many conformational changes can be described by a combination of sheer and hinge-type motions [35, 36]. Sheer-type motions involve the sliding of protein fragments (e.g., subunits or domains) over a continuously maintained interface; the change involves small, localized motion of many residues. In hinge-type motions, there is no continuously maintained interface; instead, the fragments rotate around an axis passing through a hinge region that connects the two. Hinge-type motion involves the large motion of a few residues. Another, less frequently observed, motion is the partial refolding of the protein [36]. Simple conformational changes that involve loop motions take place on the nanosecond time scale, while large changes that involve the rearrangement of domains may occur on the microsecond to millisecond time scale [37]. For some proteins, a pre-existing equilibrium of all conformational intermediates (the conformational substates) is observed [37–40]. Binding of the effector molecule shifts the population of each state, inducing the conformational change. The existence of the equilibrium suggests that the substates are separated by energy barriers of a few kcal/mol [38]. For other proteins not all species are present in the pre-existing equilibrium, e.g., for maltose-binding

protein the closed state conformer appears to be unstable in the apo form and present only when maltose is bound [41].

In observing the transformation of the hemoglobin crystals, Felix Haurowitz [1] wondered how the binding of oxygen (with a molecular weight of 32 Da) could change the shape of the hemoglobin molecules (with a molecular weight of about 64,000 Da). His question became one of the most fundamental challenges of molecular biology: how do conformational changes work? How are they induced, how are they propagated and how are they used? Intense research for 70 years has (partly) answered these questions for hemoglobin [2], but for most systems, many mysteries remain.

Computer simulations are playing an important role in elucidating the nature of the conformational transitions. First, they facilitate the interpretation of experimental data, e.g., in the classification of the motion (hinge, sheer). Second, they complement experiments by providing properties that are hard to measure experimentally, e.g., the transition pathways. The dynamic nature of conformational changes naturally lends itself to study by molecular dynamics (MD) simulation techniques. The high spatial resolution of MD (the position of each simulated atom is known at all instants) is unmatched by any experimental technique; this, in principle, would allow for a very detailed description of conformational transitions. In addition, the method may give insights into the energetics of the transition and identify the interactions responsible for the motion.

In this perspective, I will give an overview of popular atomistic techniques for the simulation of conformational transitions. The main focus will be on MD, but a few other methods will be discussed as well, including linear interpolations, normal mode analysis and minimum energy path techniques. The simulation of the GroEL chaperone will be discussed in more detail as an illustrative example. Simulations have addressed two important questions concerning the pathway and the function of the conformational transition for this large protein. Readers should note that promising coarse-grained methods, such as those related to the elastic network model [42–44], are outside the scope of this article. I will conclude with some thoughts for the future directions of this exciting field.

2 Computational methods

2.1 Interpolation schemes

The identification of a conformational change between two conformers is facilitated by interpolation methods that determine the site and type of motion. These methods assume that the transition can be described by rigid body motion of protein fragments and identify the moving parts by overlays of the structures. The transition may then be described by screw motion around a unique axis [45] or decomposed into sheer and hinge-type motions [35,36]. The pathway can subsequently be obtained by performing linear interpolations of the motion. Steric clashes along the pathway can be avoided by performing energy minimizations on each of the intermediates [35,36]. Since the sequence of motion cannot be determined by interpolation techniques, the pathways obtained in this way may not be very reliable (especially for transitions involving complex motions). For example, in the case of GroEL, linear interpolations result in a pathway in which the three domains of GroEL move in a highly concerted fashion [46]. EM experiments have shown that there is first a downward motion of the intermediate domain before significant displacements of the other two domains [47] (which was predicted by targeted molecular dynamics (TMD) simulations [48]), showing that the GroEL transition cannot be described by a linear interpolation.

2.2 Normal mode analysis

Important insights into the motion involved in a conformational change can be obtained from a normal mode analysis [49,50]. This method assumes that the energy surface in the neighborhood of the minimum energy configuration is parabolic (harmonic). The motion around the minimum can then be described by normal modes, the oscillating concerted motions of a collection of atoms. The normal modes are obtained from diagonalization of the mass-weighted Hessian H:

$$H\Psi = \Psi\Omega, \tag{1}$$

where the normal modes Ψ_i are given by the columns of the eigenvector matrix Ψ and Ω is a diagonal matrix of angular frequencies ω_i. Conformational changes are associated with the lowest frequency modes, since these modes show the largest displacements (the mean-square fluctuation of each mode is given by $k_\mathrm{b}T/\omega_i^2$). In reality, the energy surface around the minimum is not harmonic. Some of the anharmonicity may be captured by quasiharmonic analysis, in which the collective motions (the principal components) are obtained from diagonalization of the variance–covariance matrix of atomic fluctuations [49,50]. The atomic fluctuations are calculated from molecular dynamics simulations; an important advantage is that the solvent may be modeled explicitly.

The required diagonalization, which scales cubically in memory and time, is a computational bottleneck in the calculation of normal modes or principal components. Some recent advances include the development of block normal mode algorithms, in which the low-frequency modes are approximated by rigid body motion of blocks of consecutive residues [51,52]. The full diagonalization can then be replaced by the diagonalization of a much smaller residue-based matrix, enabling the treatment of very large systems. The modes obtained this way seem to agree reasonably well with the low-frequency modes obtained from a full diagonalization.

The variance–covariance matrix of atomic fluctuations is also central in a linear response theory treatment of ligand-induced conformational changes [53]. This method approximates the change in coordinate upon ligand binding Δr_i by

$$\Delta r_i = \frac{1}{k_\mathrm{b}T}\sum_j \langle \Delta r_i \Delta r_j \rangle_0 F_j, \tag{2}$$

where $\langle \Delta r_i \Delta r_j \rangle_0$ is the variance–covariance matrix in the ligand-free state and F_j the force acting on atom j due to the ligand. Applications of the method to ferric-binding protein, citrate synthase and F_1-ATPase resulted in conformational transitions that were in agreement with experiments [53].

2.3 Minimum energy path techniques

Minimum energy path techniques compute the minimum energy path connecting two conformational states ([54–62] and references therein). As an example of these methods, I will discuss the widely used conjugate peak refinement (CPR) algorithm, which yields zero temperature pathways [59]. More advanced techniques may include temperature effects and approximate classical molecular dynamics trajectories [57,60,61].

The CPR method [59] is based on the fact that the Hessian at a saddle point has exactly one negative eigenvalue: at the saddle point the energy increases in the direction of the eigenvector with the negative eigenvalue (s_0) and decreases in the direction of all other eigenvectors (s_1, s_2, ...). The saddle points are identified in an iterative way, starting with an initial guess for s_0:

$$s_0^{\mathrm{g}} = P - R, \tag{3}$$

where P and R are the coordinates for the two endstates. The energy is first maximized in the s_0^{g} direction and subsequently minimized in all directions conjugate to s_0^{g}. This yields the intermediate configuration x, from which two new guesses for s_0 are constructed ($P - x$ and $R - x$). Repetition of the procedure for each of these directions yields new intermediates, etc., ultimately converging into the true saddle points. The minimum energy path can then be obtained from steepest descent minimizations that start at the saddle points. The method requires only the energy and the gradient; the Hessian is never calculated. A drawback is that temperature effects cannot be included. Applications of the CPR method include a study of the calcium-induced conformational change in annexin V [63].

2.4 Molecular dynamics techniques

The main obstacle for the study of conformational changes by computer simulations is the time scale of the transition.[1] Atomistic MD simulations of proteins are limited to tens of nanoseconds [64]; this duration is generally much too short for the treatment of large conformational changes (although some fortuitous transitions have been simulated by unbiased MD, e.g., in a study of the gating mechanism of the mechanosensitive MscS channel [65]). Therefore, biasing techniques that enforce the conformational transition in time scales accessible to MD need to be introduced. Since the reaction coordinate for the transition is generally unknown before performing the simulation, many different strategies exist to bias the system towards the final state. Some methods bias the system along a predefined reaction coordinate in coordinate space [e.g., force probe and steered molecular dynamics (Sect. 2.4.5)]. Others bias the system along a more general predefined reaction coordinate, e.g., the difference in radius of gyration or the difference in protein contacts [e.g., biased molecular dynamics (Sect. 2.4.1)] or the root mean square difference [e.g., TMD (Sect. 2.4.2)]. In other techniques, the sampling is not along a predefined reaction coordinate; instead, the bias is entirely based on the energy [e.g., transition path sampling (Sect. 2.4.6) and the metadynamics technique (Sect. 2.4.7)]. In principle, such methods would result in the most reliable pathways; however, in practice, the computational expense may limit their application to low-dimensional systems.

The selection of the proper biasing technique depends on the system size and available computational resources, the existing experimental data and the properties to be studied. The system size and resources determine whether a predefined reaction coordinate should be used; experimental data on the pathway may aid the selection of the proper predefined reaction coordinate (the experimental reaction coordinate and the reaction coordinate used for the biasing should have the largest overlap). Some methods only yield transition pathways [e.g., TMD (Sect. 2.4.2)], other methods may also give (approximate) free energy profiles [e.g., force probe and steered molecular dynamics (section 2.4.5), metadynamics and accelerated dynamics (Sect. 2.4.7)]. To verify the calculated pathways, which validates whether the used biasing method was appropriate, a comparison should be made with experimental data on the intermediates (e.g., from EM), the distances between certain residues (e.g., from FRET), and residue interactions (e.g., from mutation experiments). If no experimental data are available, a combination of energetic data from the simulation and chemical intuition can be used to assess the quality of the calculated pathways.

2.4.1 Biased molecular dynamics

In the BMD method [66], a reaction coordinate is selected that connects the initial state to the final (or target) state. Typically, this reaction coordinate is a sum of intermolecular distances, e.g.,

$$\rho(t) = \frac{1}{N(N-1)} \sum_{i=1}^{N} \sum_{j \neq i}^{N} (r_{ij}(t) - r_{ij}^{\mathrm{T}})^2, \tag{4}$$

where $r_{ij}(t)$ is the distance between atom i and j at time t and r_{ij}^{T} that distance in the final state. Note that in going from the inital to the final state, $\rho(t)$ is decreased to zero. The physical potential is augmented by a half quadratic biasing potential of the form

$$W(r,t) = \begin{cases} \frac{\alpha}{2}(\rho - \rho_d)^2 & \text{if } \rho(t) > \rho_{\mathrm{d}} \\ 0 & \text{if } \rho(t) \leq \rho_{\mathrm{d}} \end{cases}, \tag{5}$$

[1] This time scale may be reduced artificially in the simulation by employing an implicit solvent model. The absence of explicit water molecules removes the friction and relaxation associated with the displacement of water molecules, speeding up the transition by orders of magnitude.

where $\rho_d(t)$ is the desired value of the reaction coordinate:

$$\rho_d(t) = \min_{0 \le \tau \le t} \rho(\tau). \tag{6}$$

When the trajectory moves towards the target ($\rho(t) < \rho_d$), the desired value of the reaction coordinate is set to that of the new configuration and the potential is left unchanged. When the trajectory moves away from the target, a non-zero bias is added to the potential, which restricts a further deviation from the target. The value of the force constant α is usually found by trial and error: when it is too small the trajectory may get stuck in an intermediate state; when it is too large the perturbation may give unphysical results. Although initially developed for protein (un)folding simulations, the method can be equally useful for the study of conformational changes. Applications of the method to the latter include the study of the γ subunit rotation of F_1-ATPase [67].

2.4.2 Targeted molecular dynamics

In the TMD method [68], the system is propagated in the presence of a physical potential and a holonomic constraint of the form

$$\Phi(\underline{X}(t)) = \sum (\underline{X}_i(t) - \underline{X}_{T_i})^2 - \underline{\rho}^2(t) = 0, \tag{7}$$

where $X_i(t)$ is the position of atom i at time t, X_T the target position, $\rho(t)$ the desired root mean square deviation (rmsd) with the target, and the sum is over all atoms. The underlines indicate that the coordinates have been scaled by $\sqrt{m_i/\langle m \rangle}$, where m_i is the mass of atom i and $\langle m \rangle$ the average atomic mass. This mass scaling removes the net translation of the system [68]. Using the leap-frog propagator [69], $X_i(t)$ is given by

$$X_i(t) = x_i(t) + p_i(t), \tag{8}$$

where $x_i(t)$ is the position in the absence of the holonomic constraint and $p_i(t)$ the perturbation due to the holonomic constraint. The perturbation can be written as a scaling factor γ times the difference between the previous position and the target:

$$p_i(t) = \gamma \left(X_i(t - \Delta t) - X_{T_i} \right). \tag{9}$$

γ is obtained from the solution of

$$a\gamma^2 + b\gamma + \Phi(\underline{x}(t)) = 0, \tag{10}$$

where

$$a = \sum \left(\underline{X}_i(t - \Delta t) - \underline{X}_{T_i} \right)^2, \tag{11}$$

$$b = 2 \sum \left(\underline{X}_i(t - \Delta t) - \underline{X}_{T_i} \right)^T \left(\underline{x}_i(t) - \underline{X}_{T_i} \right) \tag{12}$$

and

$$\Phi(\underline{x}(t)) = \sum (\underline{x}_i(t) - \underline{X}_{T_i})^2 - \underline{\rho}^2(t). \tag{13}$$

Since Eq. 10 is analytical, no iterations are needed and the constraint (Eq. 7) is exactly satisfied at each time step. To minimize the total perturbation $\sum |p_i|$, γ is chosen as the root with the lower absolute value in Eq. 10. The trajectory reaches the target structure in a predetermined number of steps by decreasing the rmsd $\rho(t) = \rho(t - \Delta t) - \Delta\rho$ with a small value of $\Delta\rho$ at each time step. To prevent rotational motion of the system, the rotation is stopped repeatedly after a chosen number of time steps [68].

The TMD method is computationally attractive, since the calculation of the perturbation is analytical and scales linearly in time and memory with the number of atoms involved. This small overhead makes the cost of a step in the TMD method nearly identical to that of the unbiased MD method. Moreover, it is a finite temperature method in which explicit solvent can be included, and it allows application of the perturbation to only a part of the system, while observing the unbiased response of the other part of interest [14]. A disadvantage of this method is that the perturbation is based on the rmsd and not on the energy. This means that large energy barriers may be crossed, which may yield (irreversible) pathways that are inaccessible to the system at normal temperatures [70]. Moreover, the method is not optimally efficient: sometimes the constraint holds back the trajectory from reaching the target [70].

Some of the recent applications of the TMD method include the study of conformational changes in GroEL [14,48], the mechanosensitive channel of *Escherichia coli* [71], plasminogen activator inhibitor 1 [72], α-chymotrypsin [73] and aspartate transcarbamylase [74].

2.4.3 Restrained targeted molecular dynamics

In a variant of the TMD method, the system is subjected to a harmonic restraint of the form

$$W = \frac{k}{2} \left(\rho(t) - \tilde{\rho}(t) \right)^2, \tag{14}$$

where $\tilde{\rho}(t)$ is the desired rmsd with the target and $\rho(t)$ the current rmsd with the target. The simulation is split up in windows, each with a different value for $\tilde{\rho}(t)$. Alternatively, the force constant can be increased during the run. Applications of the restrained TMD method include the study of conformational transitions in hemagglutinin [75] and Src tyrosine kinase [76].

2.4.4 Restricted perturbation-targeted molecular dynamics

Analogous to the TMD method, the restricted perturbation-targeted molecular dynamics (RP-TMD) method [70] subjects the system to the holonomic constraint of Eq. 7. In the RP-TMD method, though, the total perturbation $\sum |p_i|$ is limited to a preset value P_F, and the desired rmsd is treated as the unknown variable. Given P_F, the scaling factor γ takes the value $\pm\gamma_F$, where

$$\gamma_F = \frac{P_F}{\sum |X_i(t - \Delta t) - X_{T_i}|}. \tag{15}$$

To make the most efficient use of the perturbation, the rmsd

$$\underline{\rho}(t) = \sqrt{\sum (\underline{x}_i(t) - \underline{X}_{T_i})^2 - \Phi(\underline{x}(t))} \tag{16}$$

is minimized at each step. This means that $\Phi(\underline{x}(t)) = -a\gamma^2 - b\gamma$ (Eq. 10) should be maximized. Since $a > 0$, this yields $\gamma = +\gamma_F$ when $b < 0$, and $\gamma = -\gamma_F$ when $b > 0$. The crossing of large energy barriers can be further restricted by reducing $P_F \rightarrow P_B$ when $C < 0$. C is a measure of the alignment between the perturbation and the unperturbed force F:

$$C = \sum C_i = \sum |p_i| \cos(p_i, F_i). \tag{17}$$

For small $|p_i|$, a perturbation in the same direction as the unperturbed force ($C_i > 0$) is more favorable than a perturbation against it ($C_i < 0$), since the unperturbed force points downhill in energy ($F = -\nabla E$). The sign of C can easily be calculated *before* applying the actual perturbation, i.e., $C < 0$ only when $b < 0$ and $\sum(X_i(t - \Delta t) - X_{T_i}) \cdot F_i < 0$, or when $b > 0$ and $\sum(X_i(t - \Delta t) - X_{T_i}) \cdot F_i > 0$. The cost of this directional control is a relative increase in rmsd (the rmsd using P_F would be lower), effectively increasing the length of the simulation.

In the RP-TMD method, the unperturbed dynamics are recovered by letting $P_F \rightarrow 0$. This important feature restricts the crossing of energy barriers in the presence of the perturbation, resulting in lower energy pathways than those generated by the TMD method. The method also makes more efficient use of the perturbation than the TMD method, since the rmsd is minimized at each step. Note that the computational expense per MD step is identical in the TMD and RP-TMD methods; this cost scales linearly with the number of atoms involved. This method is currently being used for the simulation of conformational changes in proteins (A. van der Vaart and M. Karplus, to be published).

2.4.5 Force probe and steered molecular dynamics

The force probe [77] and steered molecular dynamics [78, 79] methods mimic atomic force microscopy experiments. The methods introduce a harmonic restraint with force constant K that attaches a site on the protein or ligand (x) to a reference point in space (x_0). The reference point is moved with speed v, resulting in the restraining force

$$F = K(x_0 + vt - x). \tag{18}$$

Alternatively, the reference point can be fixed while the force constant increases linearly with time:

$$F = \alpha t(x_0 - x). \tag{19}$$

From the non-equilibrium simulations the potential of mean force for the equilibrium process may, in principle, be calculated [80]. Applications of the method include a study of the γ subunit rotation of F_1-ATPase [81] and the gating mechanism of the mechanosensitive MscL channel protein [82].

2.4.6 Transition path sampling

In transition path sampling, an ensemble of trajectories connecting two conformational states is generated [58, 83]. From this ensemble, important kinetic information on the transition can be calculated, like the first-order rate constant of the transition process and the location of the transition state. The conformational states A and B, which are basins in the free energy landscape, are described by a set of order parameters (χ_1, χ_2, ..., χ_n) (e.g., dihedral angles, bond distances, interaction energies, etc.). The range of values of each of these order parameters must be unique for each basin; no value of χ_i can be the same for both basins. The order parameters are determined by a trial-and-error procedure. The population operator h_A determines if a configuration belongs to basin A:

$$h_A = \begin{cases} 1 & \text{if } \chi(t) = (\chi_1(t), \chi_2(t), ..., \chi_n(t)) \in A \\ 0 & \text{otherwise} \end{cases}. \tag{20}$$

Given an existing trajectory Ψ^0 between A and B (e.g., from a TMD simulation), a new trajectory Ψ^i can be generated. The acceptance probability of this trajectory is given by

$$P_{acc} = \min\left(1, \frac{h_A(\chi^i(0))\rho(\chi^i(0))h_B(\chi^i(t))}{h_A(\chi^0(0))\rho(\chi^0(0))h_B(\chi^0(t))}\right), \tag{21}$$

where $\rho(\chi(0))$ is the probability of the configuration at time 0 ($\rho \sim e^{-E/kT}$). Ψ^i is generated from a $t - t_i$ long MD simulation in the forward direction of time, and a t_i long MD simulation in the reverse direction of time, starting with the atomic positions from $\Psi^0(t_i)$ where t_i is a randomly chosen time. The initial momenta are obtained from a perturbation of the momenta of $\Psi^0(t_i)$. The procedure generates an ensemble of trajectories from which the transition state may be determined by evaluating the commitment probabilities (the chance that unrestrained trajectories starting at a certain configuration end up in a basin); at the transition state these probabilities are ~ 0.5 for each basin. The reaction rate can be obtained from the time correlation function $\langle h_A(0)h_B(t)\rangle / \langle h_A\rangle$. Despite the considerable computational cost of the method, transition path sampling has recently been applied to conformational transitions in two large biomolecular systems: the flipping of a cytosine residue in a three basepair DNA strand in water [84] and to the closing transition of DNA polymerase β [85]. For the latter system, a new umbrella sampling technique was developed to obtain an approximate free energy profile of the transition [85, 86].

2.4.7 Other MD techniques

Conformational transitions may be simulated by preparing the system in an unstable state and allowing it to relax during an unbiased MD simulation. This unstable state may be obtained by adding/removing the bound effector molecule, as done in a study of the pH-induced lid opening of β-lactoglobulin [87]. Simulation at elevated temperatures, while restraining the part of the protein not involved in the transition, may also provide insights into the motion [88, 89]. Since this method effectively boosts the entropic contribution to the free energy of the transition, transitions may be obtained that are not feasible at biologically relevant temperatures. In the conformational flooding method, the potential is augmented by a Gaussian term that drives the trajectory out of the minimum energy wells [90]. The flooding potential is only active

on the atoms involved in the lowest principal modes, and no directional bias is introduced by the Gaussian potential. The method has been applied to carbonmonoxy myoglobin, giving insights into the motion important for ligand escape pathways [91]. A similar idea is pursued in accelerated MD [92,93] and the metadynamics method [94,95]. In accelerated MD, a boost energy is added to the potential when the potential energy is below a certain threshold, facilitating the escape from the energy minima. The method also allows for the calculation of low-dimensional free energy profiles of the transition [92,93]. The metadynamics technique [94,95] uses an extended Lagrangian that couples the atomic system to a set of collective coordinates (e.g., dihedral angles) that describe the conformational change. A harmonic restraint keeps the collective coordinates close to the atomic coordinates; a history-dependent biasing potential is introduced to discourage the sampling of previously explored regions of phase space. This biasing potential consists of Gaussian terms that are dropped at small time intervals at the current coordinates of the trajectory. Upon convergence, the free energy surface is obtained from the sum of the Gaussian terms.

3 Applications

3.1 The GroEL chaperone

The GroEL chaperone helps proteins fold in the crowded environment of the cell [96]. GroEL is a large protein shaped like a double ring with dyad symmetry (Fig. 1a–f) [97,98]. Each ring is composed of seven identical subunits, which enclose a central cavity. Each subunit consists of three domains. The interactions between the two rings arise from the equatorial domains, which contain an ATP binding site. The smaller intermediate domains connect the equatorial and the apical domains. The apical domains form the entrance of the rings and are important for substrate binding [99]. Experiments have shown that the two seven-membered rings have large conformational changes, which alternate in the GroEL functional cycle. Motion within a ring is cooperative, while that between the rings is anti-cooperative [18]. The non-native protein substrate is first bound to one of the rings (the *cis* ring) in the closed (or t) state [100–102]. Binding of ATP to the equatorial domains of the *cis* ring triggers the expansion of the *cis* cavity through motion of the apical domains (the partly open or r′ state) [47,103–106]. The co-chaperone GroES then binds to close the top of the *cis* cavity while inducing an additional displacement of the apical domains that further enlarges the cavity (open or r″ state) [98,103–105]. This leads to the release of the substrate protein into the cavity. Hydrolysis of ATP and binding of unfolded protein and ATP to the other (*trans*) ring subsequently lead to the release of GroES, ADP and the substrate protein from the *cis* cavity [101,102]. It is believed that in many cases, several binding–release cycles are required to yield fully folded and functional protein. Each cycle takes about 15 s and consumes seven ATP molecules [107].

Although GroEL has an essential role in the folding of many proteins, it is still unclear what the chaperone system does. One hypothesis is that the major function of GroEL is to prevent aggregation by providing a shielded environment for folding. It has also been proposed that misfolded conformations of the protein substrate are partly unfolded by GroEL [96]. The unfolding could originate from the preferential binding of the unfolded state to GroEL. Alternatively, the mechanical force generated by the interactions between the protein substrate and GroEL during the opening motion in the t to r′ transition could "pull" the protein into a more unfolded state [13,96,108].

Computer simulations of the GroEL chaperone have provided important insights into the pathway of its conformational transition [106,48], the origin of the cooperativity within the rings and of anti-cooperativity between the rings [106,48], and the function of the conformational change [14].

3.2 Transition pathway

The GroEL transition is initiated by ATP binding to the *cis* ring [110]. Normal mode analysis and targeted dynamics simulations [48,106] showed that binding of ATP results in a downward twisting motion of the intermediate domain that is the trigger for the major conformational changes. The calculations showed that the intermediate domain displacement closes the ATP binding pocket, releases the apical domain to permit its upward motion and pushes downward on the equatorial domain [48,106]. These findings were confirmed by EM experiments a few years later [47]. The simulations also demonstrated that the r′ state is reached by a small upward motion and, looking down from the top of the *cis* ring, a small clockwise rotation of the apical domains. This is accompanied by a counter-clockwise twist of the equatorial domains of the *cis* ring. The r′ to r″ transition consists mainly of a further clockwise rotation and upward tilt of the apical domains. The motion was shown to be highly cooperative within the *cis* ring, due to steric and electrostatic effects [48]. The steric effects are due to van der Waals repulsions, which can be avoided only by a concerted motion of the seven subunits in the *cis* ring. The electrostatic effects involve an intra-ring, intersubunit salt bridge between Glu386 and Arg197, which is broken by the intermediate domain motion, in accord with EM data (Fig. 1c, d) [47]. Anti-cooperativity between the rings is primarily due to steric effects. The twisting of the equatorial domains upon ATP binding would result in severe van der Waals clashes if binding occurred in both rings [48]. Overall, the observed allosteric pathway is the result of coupled tertiary structure changes, rather than quaternary structural effects [106].

3.3 Mechanical unfolding

To investigate whether active unfolding can occur as part of the GroEL cycle, the opening transition of the *cis* ring was

simulated in the presence of denatured rhodanese as the substrate [14]. The study concentrated on the transition from the closed to r′ state, before the protein was released into the *cis* cavity, since this is the most likely phase for an unfolding interaction to occur in the GroEL cycle. Each step in the opening motion of the apical domains was induced by TMD and followed by a 10 times longer relaxation phase in which the protein substrate was allowed to respond to the change in the interactions. Only the apical domains of the GroEL *cis* ring were included in the calculations, and an implicit solvent model was employed [111]. In total, seven simulations were performed; in addition, one simulation was repeated using a 10 times longer relaxation phase. The simulations showed that during the transition, interactions between the apical domains of GroEL and the bound rhodanese substrate exert a force on rhodanese that lead to partial unfolding (Fig. 1g, h). Two factors were found to be important in the generation of the stretching force. The first was the presence of strong contacts between GroEL and the bound protein that continued to exist for a considerable portion of the transition. The second factor was the interaction of the protein substrate with multiple apical domains; it was the relative motion of several apical domains that pulled apart the rhodanese substrate.

The H and I helices of the apical domains were shown to play the primary role in accordance with the suggestions based on mutation studies [99] and peptide-bound X-ray structures [98, 112, 113]. During the first part of the transition the stretching force was mostly generated by the residues in the center of the H and I helices. The binding of rhodanese to these residues closely resembled the binding of GroES [98] and peptides [112, 113] to the apical domains in the available crystal structures. Analysis of the interaction energy and the buried binding surface revealed the importance of hydrophobic contacts. During the second part of the transition, hydrogen bonding became more important for the unfolding force, in agreement with suggestions based on the comparison of the cavity lining in the closed and open states [98]. In some of the simulations, the unfolding diminished or stopped when contacts with non-neighboring subunits were broken and contacts with only two or three neighboring subunits were present. To unfold the rhodanese substrate, it had to be "attached" to one part of GroEL and pulled by another part. This was done most effectively by spatially separated (non-neighboring) subunits. When rhodanese interacted with only two or three neighboring subunits, it was merely displaced by the forces involved and did not unfold. The importance of multidomain contacts for substrate binding is in agreement with a study of the binding of rhodanese to mutated GroEL molecules [114].

The biological role of the active unfolding may be the resetting of the starting conformation for spontanous folding. Stretching of the protein could eliminate structure elements that are trapped in a particularly misfolded conformation. The removal of intraprotein contacts and the increase of solvent-accessible surface area could facilitate the spontaneous refolding process after release into the cavity or in solution.

4 Conclusion and outlook

Atomistic simulations can greatly enhance our understanding of conformational transitions. As illustrated by the calculations on the GroEL chaperone, simulations can provide detailed insights into the transition pathways, the interactions involved and the biological function of the transition. Limitations in the time scale accessible to simulation techniques can be overcome by the application of biases that drive the trajectory from one conformation to the other. In addition, the transition may be sped up by the use of implicit solvent models.

Now that the usefulness and feasibility of MD simulations for the study of conformational changes is established, research needs to be done to enhance the accuracy of the calculations, expand the capabilities of the methods and extend the application of the methods to more systems. New methods should first be tested on small systems for which the free energy surface is known, to establish the quality of the calculated pathways (e.g., see Ref. [70]). To assess the accuracy of the methods for larger systems, it is crucial that comparisons are made with the existing experimental data. If possible, the structure of intermediates along the pathway should be verified with experimental data (e.g., from EM), as well as the distances between certain residues (e.g., from FRET or NMR data). Key interactions should be checked with the data available from mutation experiments. If available, the experimental data could even be used as restraints in the simulation (e.g., analogous to what was done in Refs. [115, 116]).

To extend the usefulness of the methods, attention should be shifted from a qualitative description towards a quantitative analysis of the pathways. In particular, emphasis should be given to the calculation of accurate free energy profiles along the pathways (e.g., with methods like Ref. [117]). These profiles would unambiguously identify all intermediates and bottlenecks in the transition; a subsequent free energy component analysis [118] along the path could, in principle, quantify the interactions involved. Given that most conformational changes involve a limited number of moving residues [35], there is hope that the calculation of accurate free energy profiles is actually feasible with present-day computers.

Given the large number of proteins for which conformational changes are important, many interesting applications remain to be performed. Simulations may help understand each individual system and aid in the grouping of systems into broader classes of proteins with similar conformational behavior. This may ultimately help to answer deeper questions concerning how conformational changes evolved as the prime means for biomolecular communication.

Acknowledgements I thank Prof. Martin Karplus and Prof. Kenneth M. Merz Jr. for their excellent guidance and continuous support. I also thank the members of their groups for many stimulating discussions. The critical comments and suggestions of Drs. Ylce Irizarry, Giorgio Colombo, Paul Maragakis and Prof. Martin Karplus on the manuscript are gratefully acknowledged. The material in the application to GroEL

is from Ref. [14]. Some of the research reviewed in this article was sponsored by a Marie Curie individual fellowship.

References

1. Haurowitz F (1938) Das Gleichgewicht zwischen Hämoglobin und Sauerstoff. Z Physiol Chem 54:266–274
2. Perutz MF, Wilkinson AJ, Paoli M, Dodson GG (1998) The stereochemical mechanism of the cooperative effects in hemoglobin revisited. Annu Rev Biophys Biomol Struct 27:1–34
3. Quiocho FA, Ledvin PS (1996) Atomic structure and specificity of bacterial periplasmic receptors for active transport and chemotaxis: variation on common themes. Mol Microbiol 20:17–25
4. Hammes GG (2002) Multiple conformational changes in enzyme catalysis. Biochemistry 41:8221–8228
5. Benkovic SJ, Hammes-Schiffer S (2003) A perspective on enzyme catalysis. Science 301:1196–1202
6. Huse M, Kuriyan J (2002) The conformational plasticity of protein kinases. Cell 109:275–282
7. Doyle DA (2004) Structural changes during ion channel gating. Trends Neurosci 27:298–302
8. Swartz KJ (2004) Towards a structural view of gating in potassium channels. Nature Rev Neurosci 5:905–916
9. Woolley GA, Lougheed T (2003) Modeling ion channel regulation. Curr Opin Chem Biol 7:710–714
10. Mallik R, Gross SP (2004) Molecular motors: strategies to get along. Curr Biol 14:R971–R982
11. Schliwa M, Woehlke G (2003) Molecular motors. Nature 422:759–765
12. Karplus M, Gao YQ (2004) Biomolecular motors: the F_1-ATPase paradigm. Curr Opin Struct Biol 14:250–259
13. Shtilerman M, Lorimer GH, Englander SW (1999) Chaperonin function: folding by forced unfolding. Science 284:822–825
14. van der Vaart A, Ma J, Karplus M (2004) The unfolding action of GroEL on a protein substrate. Biophys J 87:562–573
15. Monod M, Wyman J, Changeux JP (1965) On the nature of allosteric transitions—a plausible model. J Mol Biol 12:88–118
16. Koshland DE, Némethy G, Filmer D (1966) Comparison of experimental binding data and theoretical models in proteins containing subunits. Biochemistry 5:365–385
17. Fersht AR, Mulvey RS, Koch GLE (1975) Ligand binding and enzymic catalysis coupled through subunits in tyrosyl-tRNA synthetase. Biochemistry 14:13–18
18. Yifrach O, Horovitz A (1995) Nested cooperativity in the ATPase activity of the oligomeric chaperonin GroEL. Biochemistry 34:5303–5308
19. Davenport RC, Bash PA, Seaton BA, Karplus M, Petsko GA, Ringe D (1991) Structure of the triosephosphate isomerase-phosphoglycolohydroxamate complex: an analogue of the intermediate on the reaction pathway. Biochemistry 30:5821–5826
20. Wall ME, Gallagher SC, Trewhella J (2000) Large-scale shape changes in proteins and macromolecular complexes. Annu Rev Phys Chem 51:355–380
21. Saibil HR (2000) Conformational changes studied by cryo-electron microscopy. Nat Struct Biol 9:711–714
22. Frank J (2002) Single-particle imaging of macromolecules by cryo-electron microscopy. Annu Rev Biophys Biomol Struct 31:303–319
23. Kay LE (1998) Protein dynamics from NMR. Nat Struct Biol 5:513–517
24. Palmer AG, Kroenke CD, Loria JP (2003) Nuclear magnetic resonance methods for quantifying microsecond-to-millisecond motions in biological macromolecules. Methods Enzymol 13:748–757
25. Parak FG (2003) Proteins in action: the physics of structural fluctuations and conformational changes. Curr Opin Struct Biol 13:552–557
26. Schotte F, Lim MH, Jackson TA, Smirnov AV, Soman J, Olson JS, Phillips GN, Wulff M, Anfinrud PA (2003) Watching a protein as it functions with 150-ps time-resolved X-ray crystallography. Science 300:1944–1947
27. Cai X, Dass C (2003) Conformational analysis of proteins and peptides. Curr Org Chem 7:1841–1854
28. Clausen-Schaumann H, Seitz M, Krautbauer R, Gaub HE (2000) Force spectroscopy with single bio-molecules. Curr Opin Chem Biol 4:524–530
29. Engel A, Müller DJ (2000) Observing single biomolecules at work with the atomic force microscope. Nat Struct Biol 7:715–718
30. Haustein E, Schwille P (2004) Single-molecule spectroscopic methods. Curr Opin Struct Biol 14:531–540
31. Heyduk T (2002) Measuring protein conformational changes by FRET/LRET. Curr Opin Biotech 13:292–296
32. Doniach S (2001) Changes in biomolecular conformation seen by small angle X-ray scattering. Chem Rev 101:1763–1778
33. Sawaya MR, Kraut J (1997) Loop and subdomain movements in the mechanism of Escherichia coli dihydrofolate reductate: crystallographic evidence. Biochemistry 36:586–603
34. Bullough PA, Hughson FM, Skehel JJ, Wiley DC (1994) Structure of influenza haemagglutinin at the pH of membrane fusion. Nature 371:37–43
35. Gerstein M, Lesk AM, Chothia C (1994) Structural mechanisms for domain movements in proteins. Biochemistry 33:6739–6749
36. Gerstein M, Krebs W (1998) A database of macromolecular motions. Nucleic Acids Res 26:4280–4290
37. Kern D, Zuiderweg ERP (2003) The role of dynamics in allosteric regulation. Curr Opin Struct Biol 13:748–757
38. Frauenfelder H, Parak F, Young RD (1988) Conformational substates in proteins. Ann Rev Biophys Biophys Chem 17:451–479
39. Gunasekaran K, Ma BY, Nussinov R (2004) Is allostery an intrinsic property of all dynamic proteins? Proteins 57:433–443
40. Elber R, Karplus M (1987) Multiple conformational states of proteins: a molecular dynamics analysis of myoglobin. Science 235:318–321
41. Millet O, Hudson RP, Kay LE (2003) The energetic cost of domain reorientation in maltose-binding protein as studied by NMR and fluorescence spectroscopy. Proc Natl Acad Sci USA 100:12700–12705
42. Tirion MM (1996) Large amplitude elastic motions in proteins from a single-parameter, atomic analysis. Phys Rev Lett 77:1905–1908
43. Bahar I, Atilgan AR, Erman B (1997) Direct evaluation of thermal fluctuations in proteins using a single-parameter harmonic potential. Fold Des 2:173–181
44. Maragakis P, Karplus M (2005) Large amplitude conformational change in proteins with a plastic network model: adenylate kinase. J Mol Biol 352:807–822
45. Hayward S, Berendsen HJC (1998) Systematic analysis of domain motions in proteins from conformational change: new results on citrate synthase and T4 lysozyme. Proteins 30:144–154
46. Krebs WG, Gerstein M (2000) The morph server: a standardized system for analyzing and visualizing macromolecular motions in a database framework. Nucleic Acids Res 28:1665–1675
47. Ranson NA, Farr GW, Roseman AM, Gowen B, Fenton WA, Horwich AL, Saibil HR (2001) ATP-bound states of GroEL captured by cryo-electron microscopy. Cell 107:869–879
48. Ma J, Sigler PB, Xu Z, Karplus M (2000) A dynamic model for the allosteric mechanism of GroEL. J Mol Biol 302:303–313
49. Hayward S, Go N (1995) Collective variable description of native protein dynamics. Annu Rev Phys Chem 46:223–250
50. Berendsen HJC, Hayward S (2000) Collective protein dynamics in relation to function. Curr Opin Struct Biol 10:165–169
51. Tama F, Gadea FX, Marques O, Sanejouand Y-H (2000) Building-block approach for determining low-frequency normal modes of macromolecules. Proteins 41:1–7
52. Li G, Cui Q (2002) A coarse-grained normal mode approach for macromolecules: an efficient implementation and application to Ca^{2+}-ATPase. Biophys J 83:2457–2474

53. Ikeguchi M, Ueno J, Sato M, Kidera A (2005) Protein structural change upon ligand binding: linear response theory. Phys Rev Lett 94:078102
54. Berkowitz M, Morgan JD, McCammon JA (1983) Diffusion-controlled reactions: a variational formula for the optimum reaction coordinate. J Chem Phys 79:5563–5565
55. Elber R, Karplus M (1987) A method for determining reaction paths in large molecules: application to myoglobin. Chem Phys Lett 139:375–380
56. Czerminski R, Elber R (1990) Reaction path study of conformational transitions in flexible systems: application to peptides. J Chem Phys 92:5580–5601
57. Elber R, Cárdenas A, Ghosh A, Stern HA (2003) Bridging the gap between long time trajectories and reaction pathways. Adv Chem Phys 126:93–129
58. Pratt LR (1986) A statistical method for identifying transition states in high dimensional problems. J Chem Phys 85:5045–5048
59. Fischer S, Karplus M (1992) Conjugate peak refinement: an algorithm for finding reaction paths and accurate transition-states in systems with many degrees of freedom. Chem Phys Lett 194:252–261
60. Huo S, Straub JE (1997) The MaxFlux algorithm for calculating variationally optimized reaction paths for conformational transitions in many body systems at finite temperature. J Chem Phys 107:5000–5006
61. Passerone D, Ceccarelli M, Parrinello M (2003) A concerted variational strategy for investigating rare events. J Chem Phys 118:2025–2032
62. Quapp W (2003) Reduced gradient methods and their relation to reaction paths. J Theor Comp Chem 2:385–417
63. Santos JSO, Fischer S, Guilbert C, Lewit-Bentley A, Smith JC (2000) Pathway for large-scale conformational change in annexin V. Biochem 39:14065–14074
64. Karplus M, McCammon JA (2002) Molecular dynamics simulations of biomolecules. Nat Struct Biol 9:646–652 (with corrigenda in Nature Struct Biol 10:788-788, 2002)
65. Sotomayor M, Schulten K (2004) Molecular dynamics study of gating in the mechanosensitive channel of small conductance MscS. Biophys J 87:3050–3065
66. Paci E, Karplus M (1999) Forced unfolding of fibronectin type 3 modules: an analysis by biased molecular dynamics simulations. J Mol Biol 288:441–459
67. Ma J, Flynn TC, Cui Q, Leslie AGW, Walker JE, Karplus M (2002) A dynamic analysis of the rotation mechanism for conformational change in F_1-ATPase. Structure 10:921–931 (with erratum in Structure 10:1285–1285, 2002)
68. Schlitter J, Engels J, Krüger P, Jacoby E, Wollmer A (1993) Targeted molecular dynamics simulation of conformational change – application to the T $\leftrightarrow$ R transition in insulin. Mol Sim 10:291–308
69. Allen MP, Tildesley DJ (1987) Computer simulation of liquids. Oxford University Press, New York
70. van der Vaart A, Karplus M (2005) Simulation of conformational transitions by the restricted perturbation-targeted molecular dynamics method. J Chem Phys 122:114903
71. Kong YF, Shen YF, Warth TE, Ma J (2002) Conformational pathways in the gating of Escherichia coli mechanosensitive channel. Proc Natl Acad Sci USA 99:5999–6004
72. Krüger P, Verheyden S, Declerck PJ, Engelborghs Y (2001) Extending the capabilities of targeted molecular dynamics: simulation of a large conformational transition in plasminogen activator inhibitor 1. Protein Sci 10:798–808
73. Matrai J, Verheyden G, Krüger P, Engelborghs Y (2004) Simulation of the activation of alpha-chymotrypsin: analysis of the pathway and role of the propeptide. Protein Sci 13:3139–3150
74. Roche O, Field MJ (1999) Simulations of the T $\leftrightarrow$ R conformational transition in aspartate transcarbamylase. Protein Eng 12:285–295
75. Madhusoodanan M, Lazaridis T (2003) Investigation of pathways for the low-pH conformational transition in influenza hemagglutinin. Biophys J 84:1926–1939
76. Mendieta J, Gago F (2004) In silico activation of Src tyrosine kinase reveals the molecular basis for intramolecular autophosphorylation. J Mol Graph Model 23:189–198
77. Grubmüller H, Heymann B, Tavan P (1996) Ligand binding: molecular mechanics calculation of the streptavidin-biotin rupture force. Science 271:997–999
78. Isralewitz B, Baudry J, Gullingsrud J, Kosztin D, Schulten K (2001) Steered molecular dynamics investigations of protein function. J Mol Graph 19:13–25
79. Isralewitz B, Gao M, Schulten K (2001) Steered molecular dynamics and mechanical functions of proteins. Curr Opin Struct Biol 11:224–230
80. Park S, Khalili-Araghi F, Tajkhorshid E, Schulten K (2003) Free energy calculation for steered molecular dynamics simulations using Jarzynski's equality. J Chem Phys 119:3559–3566
81. Böckmann RA, Grubmüller H (2002) Nanoseconds molecular dynamics simulation of primary mechanical energy transfer steps in F_1-ATP synthase. Nat Struct Biol 9:198–202
82. Gullingsrud J, Schulten K (2003) Gating of MscL studied by steered molecular dynamics. Biophys J 85:2087–2099
83. Bolhuis PG, Chandler D, Dellago C, Geissler PL (2002) Transition path sampling: throwing ropes over rough mountain passes, in the dark. Annu Rev Phys Chem 53:291–318
84. Hagan MF, Dinner AR, Chandler D, Chakraborty AK (2003) Atomistic understanding of kinetic pathways for single base-pair binding and unbinding in DNA. Proc Natl Acad Sci USA 100:13922–13927
85. Radhakrishnan R, Schlick T (2004) Orchestration of cooperative events in DNA synthesis and repair mechanism unraveled by transition path sampling of DNA polymerase β's closing. Proc Natl Acad Sci USA 101:5970–5975
86. Radhakrishnan R, Schlick T (2004) Biomolecular free energy profiles by a shooting/umbrella sampling protocol, "BOLAS". J Chem Phys 121:2436–2444
87. Fogolari F, Moroni E, Wojciechowski M, Baginski M, Ragona L, Molinari H (2005) MM/PBSA analysis of molecular dynamics simulations of bovine β-lactoglobulin: free energy gradients in conformational transitions? Proteins 59:91–103
88. Bruccoleri RE, Karplus M (1990) Conformational sampling using high-temperature molecular-dynamics Biopolymers 29:1847–1862
89. Joseph D, Petsko GA, Karplus M (1990) Anatomy of a conformational change: hinged "lid" motion of the triosephosphate isomerase loop. Science 249:1425–1428
90. Grubmüller H (1995) Predicting slow structural transitions in macromolecular systems: conformational flooding. Phys Rev E 52:2893–2906
91. Schulze BG, Grubmüller H, Evanseck JD (2000) Functional significance of hierarchical tiers in carbonmonoxy myglobin: conformational substates and transitions studied by conformational flooding simulations J Am Chem Soc 122:8700–8711
92. Hamelberg D, Mongan J, McCammon JA (2004) Accelerated molecular dynamics: a promising and efficient simulation method for biomolecules. J Chem Phys 120:11919–11929
93. Hamelberg D, Shen T, McCammon JA (2005) Phosphorylation effects on cis/trans isomerization and the backbone conformation of serine-proline motifs: accelerated molecular dynamics. J Am Chem Soc 127:1969–1974
94. Laio A, Parrinello M (2002) Escaping free-energy minima. Proc Natl Acad Sci USA 99:12562–12566
95. Iannuzzi M, Laio A, Parrinello M (2003) Efficient exploration of reactive potential energy surfaces using Car-Parrinello molecular dynamics Phys Rev Lett 90:238302–238305
96. Thirumalai D, Lorimer GH (2001) Chaperonin-mediated protein folding. Annu Rev Biophys Biomol Struct 30:245–269
97. Boisvert DC, Wang J, Otwinowski Z, Horwich AL, Sigler PB (1996) The 2.4 Å crystal structure of the bacterial chaperonin GroEL complexed with ATPγS. Nat Struct Biol 3:170–177
98. Xu Z, Horwich AL, Sigler PB (1997) The crystal structure of the asymmetric GroEL-GroES-$(ADP)_7$ chaperonin complex. Nature 388:741–750

99. Fenton WA, Kashi Y, Furtak K, Horwich AL (1994) Residues in chaperonin GroEL required for polypeptide binding and release. Nature 371:614–619
100. Weissman JS, Rye HS, Fenton WA, Beechem JM, Horwich AL (1996) Characterization of the active intermediate of a GroEL-GroES-mediated protein folding reaction Cell 84:481–490
101. Rye HS , Burston SG, Fenton WA, Beechem JM, Xu Z, Sigler PB, Horwich AL (1997) Distinct actions of *cis* and *trans* ATP within the double ring of the chaperonin GroEL. Nature 388:792–798
102. Rye HS, Roseman AM, Chen S, Furtak K, Fenton WA, Saibil HR, Horwich AL (1999) GroEL-GroES cycling: ATP and nonnative polypeptide direct alternation of folding-active rings. Cell 97:325–338
103. Chen S, Roseman AM, Hunter AS, Wood SP, Burston SG, Ranson NA, Clarke AR, Saibil HR (1994) Location of a folding protein and shape changes in GroEL–GroES complexes imaged by cryo-electron microscopy. Nature 371:261–264
104. Roseman AM, Chen S, White H, Braig K, Saibil HR (1996) The chaperonin ATPase cycle: mechanism of allosteric switching and movements of substrate-binding domains in GroEL. Cell 87:241–251
105. Llorca O, Marco S, Carrascosa JL, Valpuesta JM (1997) Conformational changes in the GroEL oligomer during the functional cycle. J Struct Biol 118:31–42
106. Ma J, Karplus M (1998) The allosteric mechanism of the chaperonin GroEL: a dynamic analysis. Proc Natl Acad Sci USA 95:8502–8507
107. Todd MJ, Viitanen PV, Lorimer GH (1994) Dynamics of the chaperonin ATPase cycle: implications for facilitated protein folding. Science 265:659–666
108. Wang J, Boisvert DC (2003) Structural basis for GroEL-assisted protein folding from the crystal structure of $(GroEL\text{-}KMgATP)_{14}$ at 2.0 Å resolution. J Mol Biol 327:843–855
109. Humphrey W, Dalke A, Schulten K (1996) VMD - Visual molecular dynamics. J Mol Graphics 14:33–38
110. Inobe T, Makio T, Takasu-Ishikawa E, Terada TP, Kuwajima K (2001) Nucleotide binding to the chaperonin GroEL: non-cooperative binding of ATP analogs and ADP and cooperative effect of ATP. Biochim Biophys Acta 1545:160–173
111. Lazaridis T, Karplus M (1999) Effective energy function for proteins in solution. Proteins 35:133–152
112. Buckle AM, Zahn R, Fersht AR (1997) A structural model for GroEL-polypeptide recognition. Proc Natl Acad Sci USA 94:3571–3575
113. Chen L, Sigler PB (1999) The crystal structure of a GroEL/peptide complex: plasticity as a basis for substrate diversity. Cell 99:757–768
114. Farr GW, Furtak K, Rowland MB, Ranson NA, Saibil HR, Kirchhausen T, Horwich AL (2000) Multivalent binding of nonnative substrate proteins by the chaperonin GroEL. Cell 100:561–573
115. Paci E, Vendruscolo M, Dobson CM, Karplus M (2002) Determination of a transition state at atomic resolution from protein engineering data. J Mol Biol 324:151–163
116. Lindorff-Larsen K, Best RB, DePristo MA, Dobson CM, Vendruscolo M (2005) Simultaneous determination of protein structure and dynamics. Nature 433:128–132
117. Neria E, Fischer S, Karplus M (1996) Simulation of activation free energies in molecular systems. J Chem Phys 105:1902–1921
118. Gao J, Kuczera K, Tidor B, Karplus M (1989) Hidden thermodynamics of mutant proteins: a molecular dynamics analysis. Science 244:1069–1072